Use of dynamical diffraction effects on x-ray fluorescence to determine the polarity of GaP single crystals

P. Trucano
Department of Crystallography, University of Pittsburgh, Pittsburgh, Pennsylvania 15260
(Received 20 October 1975)

The dynamical theory of x-ray diffraction, which predicts a highly structured internal field intensity during symmetric Bragg reflection from large single crystals, was applied to the ± (111) and ± (222) Bragg reflections from noncentrosymmetric GaP crystals. It was shown that theory predicts an internal field intensity with maximal and minimal surfaces. At the low-angle side of the region of total reflection, the surface of maximal field intensity is positioned to sense the least amount of charge density. The field intensity moves into the crystal during the scan of the total reflection range until it senses the maximum amount of charge density at the high-angle limit of total reflection. During scans of the (111) and ($\bar{1}\bar{1}\bar{1}$) reflections, the field intensity moves across the atomic planes in different sequences so that the polarity of the crystal may be determined by monitoring the x-ray fluorescence from the phosphorus or gallium atoms. This polarity determination does not reguire an anomalously scattered component in the diffracted beam as have all previous determinations. Experimental phosphorus fluorescence profiles were obtained during diffraction of Cu $K\alpha$ radiation from the ± (111) and ± (222) reflections. The long-wavelength phosphorus $K\alpha$ radiation provided distinct advantages in detecting the internal field motion, and the ± (222) reflection profiles provided internal checks on the ± (111) results. The experimental profiles agreed with theoretical predictions and determined the GaP crystal polarity. The polarity was also determined by the traditional anomalous dispersion method using Mo $K\alpha$ radiation. The two methods gave consistent results providing experimental confirmation of the predictions of dynamical and kinematic theories of x-ray diffraction. The fluorescence technique also provides a means for determining the arrangement of atoms in crystals in a new and direct way.

INTRODUCTION

When x rays are diffracted from planes parallel to the surface of a large single crystal (symmetric Bragg case), the diffracted beam intensity is nearly equal to that of the incident beam for a small range of incident angles (typically about 10 sec of arc) called the region of total reflection. The dynamical theory of diffraction[1–3] predicts a distribution of energy inside the crystal as well as the diffracted beam intensity. Within the total reflection region the internal field intensity has periodic maximal and minimal surfaces which are parallel to the diffracting planes. The positions of these surfaces relative to the atomic planes are a function of the angle of incidence, and shift $\frac{1}{2}$ the distance separating the diffracting planes as the region of total reflection is scanned. For centrosymmetric crystals and for "full" reflections in which all atoms in the crystal scatter in phase, the internal-field intensity has distinct minima at the atom positions when the incident beam is at the low-angle limit of the range of total reflection, whereas maxima appear at the atom planes at the high-angle limit.

If the incident beam is energetic enough to fluoresce atoms in the crystal, the fluorescence intensity outside the crystal will depend on the wave-field intensity at the fluorescing atoms. Fluorescence profiles, obtained as a Bragg reflection is scanned, can therefore be used to deduce the position of the field intensity inside the crystal or, once the motion of the field intensity is understood, the profile can be used to deduce the position of the fluorescing atoms. Batterman[4] has experimentally verified the dynamical theory's prediction of the internal-field intensity, and these predictions have been used to locate the lattice positions of impurity atoms by monitoring the characteristic fluorescence of the impurities.[5,6]

Both of the above studies were done on centrosymmetric crystals utilizing so-called "full" reflections. In the work reported here, the wave field in a noncentrosymmetric crystal containing two different kinds of atoms has been examined. In such a crystal the minimal surfaces of the internal field will not necessarily be coincident with the atom positions at the onset of total reflection. Furthermore, as the wave field shifts during a scan of the total-reflection region, it can cross planes of different atomic species in a predictable sequence. This sequence may be monitored by detecting the fluorescence intensity characteristic of the various elements, and this information can, in principle, distinguish between crystal polarities without recourse to anomalous scattering effects. Experimental phosphorous fluorescence profiles from GaP single crystals during scans of the (111) and ($\bar{1}\bar{1}\bar{1}$) reflections were measured to demonstrate this new method for determining crystal polarity. Profiles for the (222) and ($\bar{2}\bar{2}\bar{2}$) reflections were also obtained to check the consistency of the experiment. GaP was chosen because light atoms provide distinct advantages in

detecting the important features of the fluorescence profiles. In previous work[4,5] the effects of primary extinction (i.e., the limiting of the x-ray penetration depth into the crystal in the total-reflection range) imposed a large dip on the fluorescence profile because fewer atoms fluoresce in this region. This dip tended to obscure the effects of the motion of the wave-field intensity, but the use of light atom fluorescence minimizes the dip as fluorescence stimulated deep inside the crystal for angles of incidence outside the total-reflection region is absorbed within the crystal before it reaches the surface. Although the total fluorescence observed outside the crystal was reduced, the effect of the wave-field motion on the observed profile was enhanced.

Although x rays have been used to determine crystal polarity and absolute configurations for over forty years, the correctness of the anomalous-dispersion technique has recently been questioned.[7] The treatment of anomalous scattering in neutron diffraction was subsequently checked and verified.[8] The fluorescence technique reported here provides an independent check on the treatment of anomalous scattering in x-ray diffraction.

THEORY

In this section the relevant aspects of dynamical theory will be reviewed and applied to the GaP structure. Several summaries of the dynamical theory have been published;[1-3] the treatment and notation here will follow that of Batterman and Cole.[3]

The total wave field $\vec{\mathcal{E}}$ inside the crystal can be expressed in terms of two plane waves, $\vec{\mathcal{E}}_0$ of amplitude $\vec{E}_0$ traveling very nearly in the incident beam direction, and $\vec{\mathcal{E}}_H$ with amplitude $\vec{E}_H$ traveling in the diffracted beam direction, where

$$\vec{\mathcal{E}}_0 = \vec{E}_0 \exp(i\omega t - 2\pi i \vec{K}_0' \cdot \vec{r}) \exp(-4\pi \vec{K}_0'' \cdot \vec{r}) , \quad (1a)$$

$$\vec{\mathcal{E}}_H = \vec{E}_H \exp(i\omega t - 2\pi i \vec{K}_H' \cdot \vec{r}) \exp(-4\pi \vec{K}_H'' \cdot \vec{r}) . \quad (1b)$$

The complex wave vectors $\vec{K} = \vec{K}' - i\vec{K}''$ include an absorptive term owing to the imaginary part $-\vec{K}''$, which is the same for both waves. To evaluate the fluorescence produced by the total wave field inside the crystal, the amplitudes and complex wave vectors of the two waves must be calculated.

The allowed wave vectors, $\vec{K}_0$ and $\vec{K}_H$, for waves inside the crystal, must originate from points on the dispersion surface defined by

$$\xi_0 \xi_H = \tfrac{1}{4} k^2 P^2 \Gamma^2 F_H F_{\bar{H}} ,$$

where $\xi_{0,H} = (\vec{K}_{0,H} \cdot \vec{K}_{0,H})^{1/2} - k(1 - \Gamma F_0)$. The wave vector of the incident radiation in vacuum is $k = 1/\lambda$. $P = 1$ and $\cos 2\theta$ for the σ and π states of polarization of the incident beam (each polarization state may be treated as a separate problem), $\Gamma = (e^2/4\pi\epsilon_0 mc^2)(\lambda^2/\pi V)$, and F_H and $F_{\bar{H}}$ are the structure factors for the reflections from planes defined by the reciprocal-lattice vectors $\vec{H}$ and $-\vec{H}$, respectively. The determination of ξ_0 also characterizes the ratio of the field amplitudes since

$$E_H / E_0 = -2\xi_0 / kP\Gamma F_{\bar{H}} . \quad (2)$$

The active points on the dispersion surface are determined by the boundary conditions including the incident beam angle and the orientation of the surface with respect to the diffracting planes. For the symmetric Bragg case

$$\xi_0 = \tfrac{1}{2} k |P| \Gamma (F_H F_{\bar{H}})^{1/2} [\eta \pm (\eta^2 - 1)^{1/2}] , \quad (3)$$

where $\eta \equiv (-\Delta\theta \sin 2\theta + \Gamma F_0)/\Gamma |P| (F_H F_{\bar{H}})^{1/2}$ and $\Delta\theta$ is the deviation from the Bragg angle.

The definition of ξ_0 implies that $\xi_0 > 0$ for active points on the α branch of the dispersion surface and $\xi_0 < 0$ for active points on the β branch. Kohler[9] has shown that points on the upper half of the α branch and lower half of the β branch lead to nonphysical solutions. Therefore, the minus sign in Eq. (3) will apply for α branch points and the positive sign for solutions on the β branch.

When $|\eta| < 1$, no points on either branch are excited but there are complex solutions for ξ_0 which provide accurate solutions for these conditions. The plus sign in Eq. (3) will lead to positive imaginary component of ξ_0 and the minus sign implies a negative imaginary component. A positive imaginary component of ξ_0 leads to an exponential increase of the incident wave inside the crystal, which is physically unacceptable. Therefore, the negative sign in Eq. (3) is appropriate for this range of incident angles.

It is convenient to parameterize η such that $\eta = \cosh u$ for $\eta > 1$, $\eta = \sin v$ for $|\eta| < 1$, and $-\eta = \cosh u$ for $\eta < -1$. The above results may be summarized

$$\xi_0 = \begin{cases} \tfrac{1}{2} k |P| \Gamma (F_H F_{\bar{H}})^{1/2} e^{-u} & \text{for } \cosh u = \eta < -1, \\ \tfrac{1}{2} k |P| \Gamma (F_H F_{\bar{H}})^{1/2} e^{iv - i\pi/2} & \text{for } -1 \le \sin v = \eta \ge 1, \\ \tfrac{1}{2} k |P| \Gamma (F_H F_{\bar{H}})^{1/2} e^{-u} & \text{for } -\cosh u = \eta > 1 . \end{cases} \quad (4)$$

The total wave field $\vec{\mathcal{E}}$ is the sum of the two fields $\vec{\mathcal{E}}_0$ and $\vec{\mathcal{E}}_H$ inside the crystal. The field intensity in the crystal will be proportional to a quantity R defined by

$$R \equiv \vec{\mathcal{E}} \cdot \vec{\mathcal{E}}^* , \quad (5)$$

where the asterisk denotes the complex conjugate. Combining Eqs. (1), (2), and (5),

$$R = |1 + (E_H/E_0) e^{2\pi i \vec{H} \cdot \vec{r}}|^2 = |1 - (2\xi_0 / kP\Gamma F_{\bar{H}}) e^{2\pi i \vec{H} \cdot \vec{r}}|^2 , \quad (6)$$

where Bragg's law relating $\vec{K}_0$ and $\vec{K}_H$ so that $\vec{K}_H - \vec{K}_0 = \vec{H}$ was used. R is constant parallel to

the diffracting planes and has the periodicity of the reflecting planes. Note that R is a function of the position $\vec{r}$ directly in the exponential and indirectly in $F_{\vec{H}}$, both of which depend on the choice of origin.

An argument owing to Batterman and Cole[3] may be used to arrive at the positions of the minimal planes of R relative to the atomic planes. These positions must be independent of the choice of origin. Let the origin of $\vec{r}$ be in one of these planes so that $e^{2\pi i \vec{H}\cdot\vec{r}} = 1$. Then to minimize R, E_H/E_0 must be minimized. They pointed out that if the crystal has a center of symmetry and if all atoms scatter in phase, nodal planes (i.e., $R = 0$) exist at the center of symmetry when $\eta = 0$. When $\eta = 1$, at the low-angle limit of the range of total reflection, the nodal surfaces are at the atoms, and when $\eta = -1$, antinodal or maximal surfaces are at the atoms.[10] For the noncentrosymmetric crystal GaP, and for a reflection in which all the atoms do not scatter in phase, the nodal planes when $\eta = 1$ are still positioned so that they sense the least amount of charge density but they are not exactly in the atom planes. When $\eta = -1$, the field is positioned to sense the maximum amount of charge density.

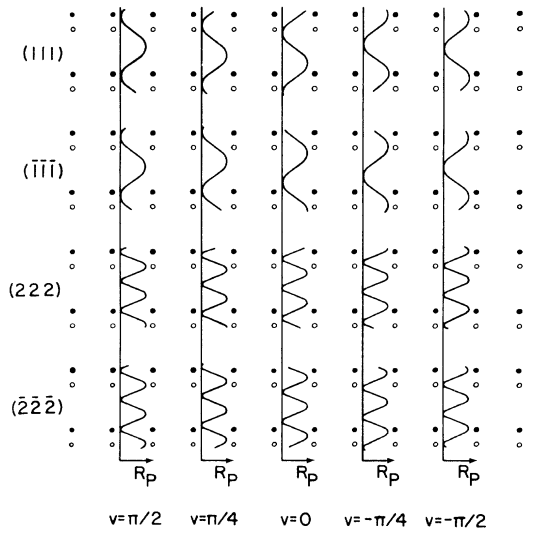

FIG. 1. Schematic illustration of the GaP structure viewed along the $[11\bar{2}]$ direction so that the [111] direction points toward the top of the figure and the $[\bar{1}\bar{1}\bar{1}]$ direction points toward the bottom. Open circles represent phosphorus atoms and solid circles represent gallium atoms. Overlaying the structural schematic are graphs of the internal field intensity R_P for five angles of incidence within the total reflection region ($v = \frac{1}{2}\pi$ corresponds to the low angle limit). Graphs show the relationship of the maximal and minimal surfaces to the atomic planes as the ±(111) and ±(222) reflections are scanned. Maximal surfaces move downward in the figure for the (111) and (222) reflections but move upward for the $(\bar{1}\bar{1}\bar{1})$ and $(\bar{2}\bar{2}\bar{2})$ reflections. This movement results in different field intensities at the phosphorous layers for the ±(111) reflections but identical intensities at the phosphorus layers for the ±(222) reflections.

Consider symmetric Bragg diffraction from the (111) planes of GaP using Cu $K\alpha$ radiation so that the imaginary terms in the atomic scattering factors f may be neglected. Then $|F_{hkl}| = |F_{\bar{h}\bar{k}\bar{l}}|$. The [111] and $[\bar{1}\bar{1}\bar{1}]$ directions are defined by positioning Ga atoms at coordinates (0, 0, 0)+fcc positions and P atoms at $(\frac{1}{4}, \frac{1}{4}, \frac{1}{4})$+fcc positions in the cubic unit cell, as shown in Fig. 1. To allow the choice of origin to be governed by the minimization of E_H/E_0, the structure factors F_{111} and $F_{\bar{1}\bar{1}\bar{1}}$ are computed for an origin at a Ga atom plus the vector $\vec{r}_t$. Then

$$F_{111} = 4(f_{Ga}^2 + f_P^2)^{1/2} \exp i[-2\pi\vec{H}_{111}\cdot\vec{r}_t - \arctan(f_P/f_{Ga})] \quad (7a)$$

and

$$F_{\bar{1}\bar{1}\bar{1}} = 4(f_{Ga}^2 + f_P^2)^{1/2} \exp i[-2\pi\vec{H}_{\bar{1}\bar{1}\bar{1}}\cdot\vec{r}_t + \arctan(f_P/f_{Ga})] . \quad (7b)$$

Substituting Eqs. (7a), 7(b), and (4) into Eq. (2) for E_H/E_0, the minimization criteria become

$$2\pi\vec{H}_{\bar{1}\bar{1}\bar{1}}\cdot\vec{r}_t = \tfrac{1}{2}\pi - v + \arctan(f_P/f_{Ga}) + 2\pi n \quad (8a)$$

for the (111) reflection, and

$$2\pi\vec{H}_{111}\cdot\vec{r}_t = \tfrac{1}{2}\pi - v - \arctan(f_P/f_{Ga}) + 2\pi n \quad (8b)$$

for the $(\bar{1}\bar{1}\bar{1})$ reflection, where n is any integer. At the low angle limit of the region of total reflection $\eta = 1$ or $v = \frac{1}{2}\pi$ and the nodal surfaces are slightly below the gallium layers in Fig. 1. As the total reflection region is traversed, v decreases to $-\frac{1}{2}\pi$ and Eqs. (8a) and (8b) indicate that the nodal surfaces move in the $[\bar{1}\bar{1}\bar{1}]$ direction for the (111) reflection ($2\pi\vec{H}_{\bar{1}\bar{1}\bar{1}}\cdot\vec{r}_t$ increasing), and in [111] direction for the $(\bar{1}\bar{1}\bar{1})$ reflection ($2\pi\vec{H}_{111}\cdot\vec{r}_t$ increasing), as shown in Fig. 1. Note that the nodal surfaces cross the phosphorus layers during the (111) scan, but not during the $(\bar{1}\bar{1}\bar{1})$ scan.

Noting the position of the phosphorus layers relative to the nodal surfaces and the sinusoidal dependence of the field intensity with position in the crystal, a function R_P proportional to the field intensity at the phosphorus layers may be formed, where

$$R_P = \begin{cases} 1 + e^{-2u} - 2e^{-u}\sin[\arctan(f_P/f_{Ga})] \\ \qquad \text{for } \eta = \cosh u > 1 , \\ 2 \mp 2\cos[v \mp \arctan(f_P/f_{Ga})] \\ \qquad \text{for } 1 \geq \eta = \sin v \geq -1 , \\ 1 + e^{-2u} + 2e^{-u}\sin[\arctan(f_P/f_{Ga})] \\ \qquad \text{for } \eta = -\cosh u < -1 , \end{cases} \tag{9}$$

where the minus signs in the second equation apply to the (111) reflection and the plus signs to the $(\bar{1}\bar{1}\bar{1})$ reflection.

The results for the ±(111) reflections may be contrasted with those for the (222) and $(\bar{2}\bar{2}\bar{2})$ reflections. In this case,

$$F_{222} = 4(f_{Ga} - f_P)e^{-2\pi i \vec{H}_{222}\cdot\vec{r}_t}$$

and

$$F_{\bar{2}\bar{2}\bar{2}} = 4(f_{Ga} - f_P)e^{-2\pi i \vec{H}_{\bar{2}\bar{2}\bar{2}}\cdot\vec{r}_t} .$$

The position of the nodal surfaces, following the same reasoning that was applied to the ±(111) reflections, will be at the Ga layers at the low angle limit of the total reflection region. As with the ±(111) reflections, the (222) nodal surfaces move in the $[\bar{2}\bar{2}\bar{2}]$ direction, and the $(\bar{2}\bar{2}\bar{2})$ nodal surfaces move in the [222] direction, as shown in Fig. 1. However, because the periodicity of the wave field intensity is twice that for the (111) reflections, the intensity at any atomic plane in the crystal is the same for the (222) and $(\bar{2}\bar{2}\bar{2})$ scans. The intensity at the phosphorus layers will be given by

$$R_P = \begin{cases} 1 + e^{-2u} + 2e^{-u} & \text{for } \eta = \cosh u > 1 , \\ 2 + 2\sin(v) & \text{for } 1 \geq \eta = \sin v \geq -1 , \\ 1 + e^{-2u} - 2e^{-u} & \text{for } \eta = -\cosh u < -1 . \end{cases} \tag{10}$$

Note that the maximal surfaces are at the phosphorus layers at the beginning of total reflection although the wave field is still located so that it senses the least amount of total charge density and moves to sense the maximum charge density at the high angle side of the total reflection region.

EXPERIMENTAL

GaP single crystals, 2 mm thick and 2 cm in diameter, with dislocation densities of ~3000 dislocations/cm^2 were used. One surface of crystal No. 1 and both front and back surfaces of crystal No. 2 were cut parallel to the (111) planes and chemically polished using sulfuric acid, peroxide, and water in the ratio 3 : 1 : 1. Care was taken to form both surfaces of crystal No. 2 equally well. One side was labeled *A* and the other *B* as the polarity was not known initially.

Figure 2 illustrates the experimental apparatus

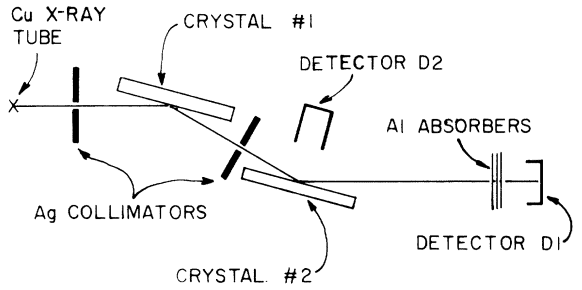

FIG. 2. Schematic of the experimental setup for recording fluorescence profiles. Detector *D*1 is a scintillation detector and *D*2 is a Si(Li) solid-state detector.

used to obtain the fluorescence profiles. Crystal No. 1 served as a monochromator for the 8.04-keV Cu $K\alpha$ x rays from the vertical x-ray tube. The Cu $K\alpha$ x rays diffracted from the (111) planes of crystal No. 1 impinged on the surface of the second crystal. Crystal No. 2 was slowly rotated about an axis perpendicular to the plane of diffraction and through the (111) reflection of the second crystal. The beam diffracted from crystal No. 2 was monitored by the diffracted beam detector. Aluminum absorbers were placed in front of this counter to prevent overloading of the counting system. As the peak was scanned, the fluorescence detector, a Si(Li) solid-state detector placed in front of the second crystal, monitored the phosphorus fluorescence. The Si(Li) detector had an energy resolution of 180 eV and the spectrum of x rays it received is shown in Fig. 3, as recorded by a multichannel analyzer. The Cu $K\alpha$ radiation in the spectrum was due primarily to Compton and thermal diffuse scattering and the Ga $K\alpha$ line was due to fluorescence from crystal No. 2 stimulated by higher-order harmonics in the incident beam. The Si $K\alpha$ line was stimulated within the detector crystal and was effectively eliminated electronically by the single-channel–analyzer discrimination indicated in Fig. 3.

The x-ray tube was run at 40 keV and 20 mA and the second crystal was continuously scanned at 0.1074 sec of arc per min. After the two crystals were aligned so that the (111) diffraction vector was in the diffracting plane and perpendicular to the axis of rotation of the second crystal, scans of approximately 300 sec of arc through the (111) reflections for side *A* and side *B* of crystal No. 2 were made. The counts accumulated by both detectors were recorded every 800 sec. The average fluorescence count rate was about 3.5 counts/sec. Six to ten scans were averaged together to produce the fluorescence profiles shown in Fig. 4. The diffracted beam profiles were

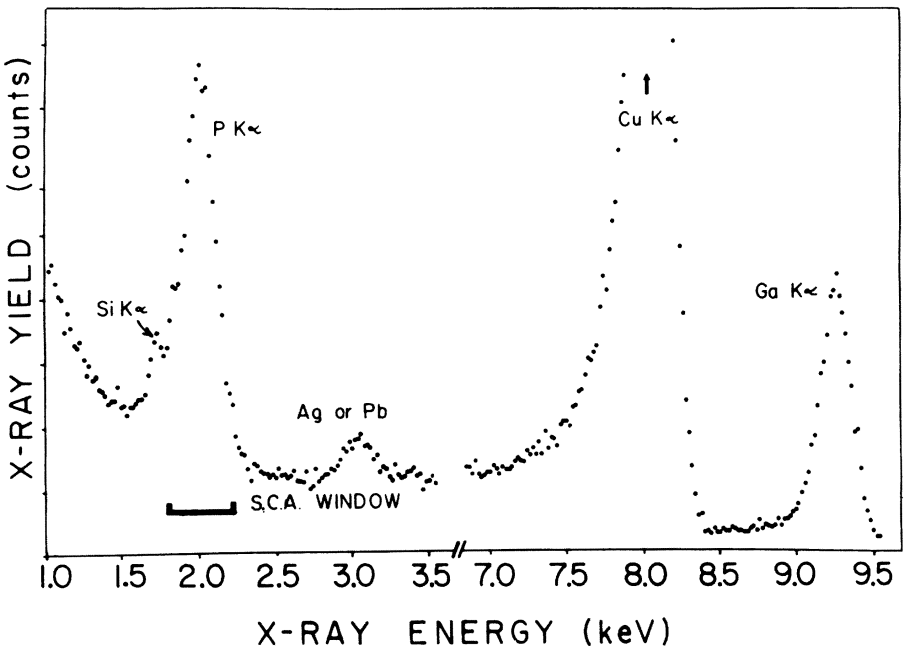

FIG. 3. Energy spectrum received by detector $D2$ as recorded by a multichannel analyzer. Characteristic peaks of Si, P, Cu, and Ga are indicated. Small peak at 3.0 keV is probably owing to the Ag or Pb in the collimation system. Window setting of the single-channel analyzer (SCA) used for recording phosphorus fluorescence is indicated. There was no structure in the spectrum between 3.5 and 7.0 keV.

used to provide an angular reference for each fluorescence profile in the averaging process. The variations in incident beam intensity were 1 to 2% with periods of from 10 to 20 h, and these variations were effectively averaged out by using 6 to 10 48-h scans to obtain the final fluorescence profiles. No effects owing to multiple reflections were observed as fluorescence profiles for several azimuthal positions were obtained by rotating crystal No. 2 about its diffraction vector.

Because only the fluorescence from atoms near the surface of crystal No. 2 contributed to the fluorescence profiles, any differences in perfection of the two surfaces could have a significant effect on the profiles obtained from side A and side B. To check for such differences in surface perfection, profiles for the (222) reflections from both sides of crystal No. 2 were obtained with crystal No. 1 set to diffract from the (222) reflection. Theory predicts that these profiles will be the same and any significant differences in surface perfection or experimental procedures in the two cases would become evident.

RESULTS

The phosphorus fluorescence profiles obtained during reflection of Cu $K\alpha$ radiation from the (111) reflections and the (222) reflections are shown in Figs. 4 and 5. The difference between the (111) profiles from side A and B was evident, and resulted from the way the internal wave field moved through the crystal in the two cases. The (111) profile from side A showed a 6% increase above the background level on the low angle side of the range of total reflection and a dip of about equal magnitude as the total reflection range was scanned. The dip in the (111) profile from side B was more than four times that from side A. It may be concluded that the maximal planes of the internal field intensity passed through the phosphorus layers during the (111) reflection from side A but did not during the side B reflection. The effects of extinction in the total reflection region tended to reduce both the observed fluorescence profiles, but the passing of the field intensity through the phosphorus layers during the side A reflection led to a smaller dip than for the side B reflection. On the basis of these results, it was concluded that the outward normal to side A was in the $[\bar{1}\bar{1}\bar{1}]$ direction and the outward normal to side B was in the [111] direction.

The profiles for the (222) reflections from side A and B were indistinguishable. In both cases the fluorescence intensity dipped on the low angle side of the total reflection range and peaked on the high angle side. The internal wave field moved so that its intensity at the phosphorus layers is the same for the (222) and $(\bar{2}\bar{2}\bar{2})$ reflections and its maximal surfaces were at the phosphorus layers at the beginning of the total reflection range.

To obtain a more quantitative measure of the agreement with theory, several experimental factors were considered. R_P, given by Eqs. (9) and (10) for the $\pm(111)$ reflection and the $\pm(222)$, respectively, is proportional to the field intensity

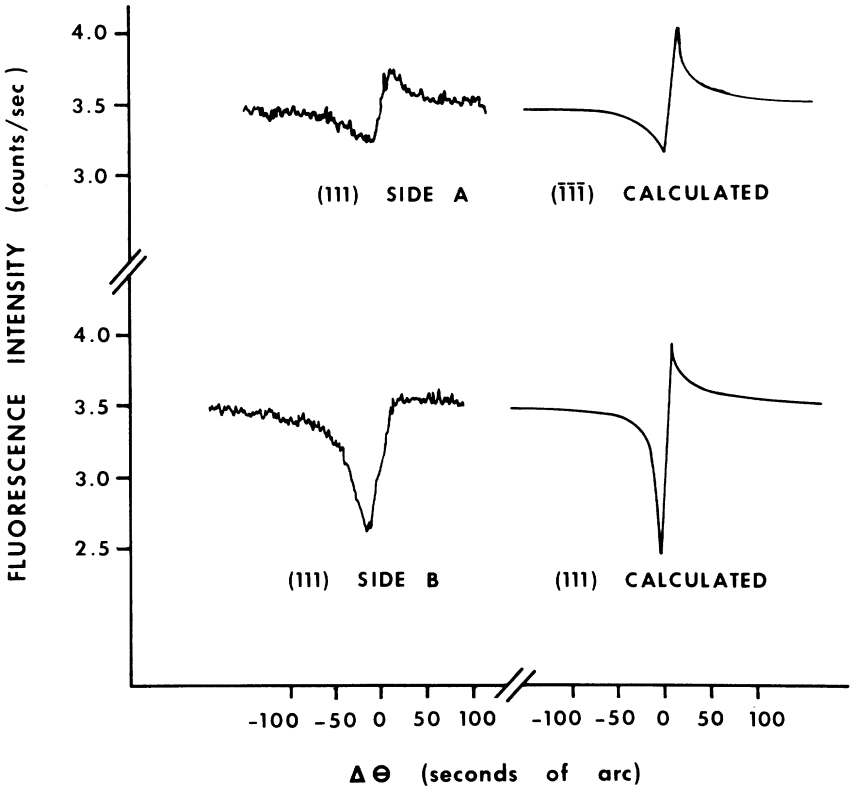

FIG. 4. Experimental phosphorus fluorescence profiles for the (111) reflection from side *A* and side *B* of the GaP crystal and the calculated profiles for the (111) and ($\bar{1}\bar{1}\bar{1}$) reflections.

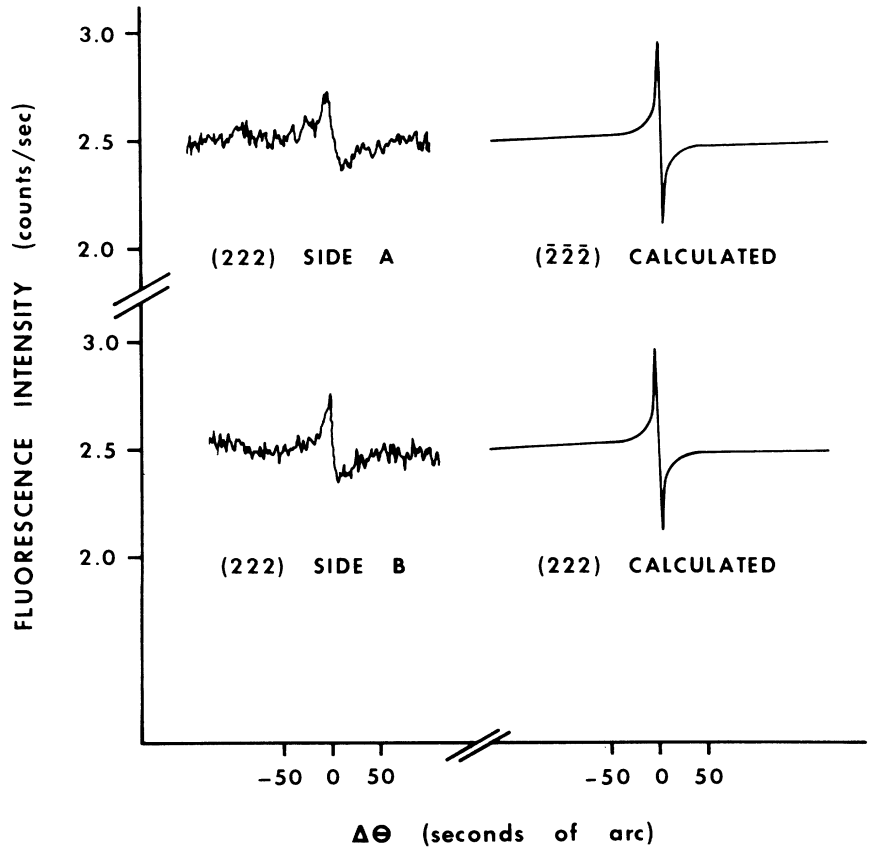

FIG. 5. Experimental phosphorus fluorescence profiles for the (222) reflection from side *A* and side *B* of the GaP crystal and the calculated profiles for the (222) and ($\bar{2}\bar{2}\bar{2}$) reflections.

at the phosphorus layers for a particular polarization of the incident beam. During total reflection, the intensity of the wave field is exponentially damped with depth into the crystal owing to the imaginary component of K_0 and K_H, that is, $K_0'' = K_H'' = -\xi_0''/\sin\theta$. The fluorescence intensity reaching the surface of the crystal is limited by GaP absorption of the phosphorus $K\alpha$ x rays. When the fluorescence intensity is detected perpendicular to the surface of the crystal, the intensity is proportional to $(\mu_l + \mu_{ext})^{-1}$ where μ_l is the linear absorption coefficient of phosphorus $K\alpha$ radiation in GaP, and

$$\mu_{ext} = \begin{cases} 0 & \text{for } |\eta| > 1 \\ -4\pi\xi_0''/\sin\theta & \text{for } |\eta| < 1 \end{cases} .$$

Another factor affecting the observed profiles is the divergence in the incident beam. Each wavelength diffracted from crystal No. 1 emerged with an angular profile T, where

$$T = |\eta \pm (\eta^2 - 1)^{1/2}|^2 .$$

The actual intensity at the phosphorus layers in the crystal will be proportional to the convolution of R_P with T.

Finally the incident beam contained two states of polarization which can be treated independently. The σ polarization in the plane of diffraction and the π polarization out of the plane of diffraction were in the ratio 1 to $\cos 2\theta$ as a result of diffraction from crystal No. 1. Taking these factors into account, the experimental profiles should be proportional to R_P^{tot} where

$$R_P^{tot} = [1/(\mu_l + \mu_{ext}^{\sigma})]R_P^{\sigma} * T^{\sigma} + [1/(\mu_l + \mu_{ext}^{\pi})]|\cos 2\theta| R_P^{\pi} * T^{\pi} , \quad (11)$$

where the stars denote convolutions. Figures 4 and 5 contain the calculated profiles obtained from Eq. (11) where the following parameters were used in the calculation: $\mu_l = 11\,727$ cm^{-1} (derived from the calculated mass absorption coefficient for 2.75-Å radiation[11] assuming a λ^3 dependence for μ_l), GaP lattice parameter $a = 5.450$ Å,[12] $\lambda = 1.542$ Å, and $|F_{111}| = 111.80$ and $|F_{222}| = 52.03$ from calculated atomic scattering factors[13,14] neglecting $\Delta f''$. The proportionality constant was determined by matching the fluorescence intensity away from the Bragg peak and fitting the calculated and measured profiles. In this manner a single proportionality constant was obtained for the $\pm(111)$ profiles and a different constant for the $\pm(222)$ profiles.

To check the fluorescence results, the polarity of the GaP crystal was determined by the traditional method of measuring integrated intensities of reflections (hkl) and $(\bar{h}\bar{k}\bar{l})$ when the diffracted beam contains a strong anomalous scattering component.[15] The intensity ratios for the $\pm(333)$, $\pm(444)$, and $\pm(555)$ reflections were measured using Mo $K\alpha$ radiation which is sufficiently energetic to produce a large anomalous scattering component from the Ga atoms. The double-crystal spectrometer shown in Fig. 2 was used with crystal No. 1 set to diffract from the (333) reflection. Integrated intensities for each of the three reflections from side A and from side B were measured, integrating over the $K\alpha_1 - K\alpha_2$ doublet for the (333) reflections but only over the $K\alpha_1$ line for the (444) and (555) reflections.

Cole and Stemple[16] have shown that the ratio of the integrated intensities $\rho_{hkl}/\rho_{\bar{h}\bar{k}\bar{l}}$ is independent of crystal perfection and is given by

$$\rho_{hkl}/\rho_{\bar{h}\bar{k}\bar{l}} = |F_{hkl}|^2/|F_{\bar{h}\bar{k}\bar{l}}|^2 . \quad (12)$$

The measured ratios and calculated ratios from Eq. (12) using theoretical values for the atomic scattering factors[13] and anomalous dispersion corrections[14] are shown in Table I. This technique verified that the perpendicular to side A corresponds to the $[\bar{1}\bar{1}\bar{1}]$ direction and to side B corresponds to the [111] direction, in agreement with the fluorescence results.

DISCUSSION

The calculated profiles contained the prominent features of their respective profiles. The reversal of the angular position of the peaks and dips for the $\pm(111)$ and $\pm(222)$ reflections was verified. Also, the relative height of the peaks and dips in the measured (111) and $(\bar{1}\bar{1}\bar{1})$ profiles agreed with the calculation. All the calculated profiles were sharper. This disparity was probably owing to the perfection of the GaP samples. The dislocation density was sufficient to cause broadening of the reflected beam profile,[17] and consequently the dynamical interactions inside the crystal took place over a larger angular range and were less strongly coupled within the region of total reflection.

The intensity ratio measurements done with Mo $K\alpha$ radiation indicated some difference in crystalline perfection on the two faces of the

TABLE I. Calculated and experimental integrated intensity ratios for the (hhh) and $(\bar{h}\bar{h}\bar{h})$ reflection pairs of GaP using Mo $K\alpha$ radiation.

Calculated	Experimental
$\rho_{333}/\rho_{\bar{3}\bar{3}\bar{3}} = 1.13$	$(\rho_{\text{side }B}/\rho_{\text{side }A})_{333} = 1.21$
$\rho_{444}/\rho_{\bar{4}\bar{4}\bar{4}} = 1.00$	$(\rho_{\text{side }B}/\rho_{\text{side }A})_{444} = 1.04$
$\rho_{555}/\rho_{\bar{5}\bar{5}\bar{5}} = 0.82$	$(\rho_{\text{side }B}/\rho_{\text{side }A})_{555} = 0.84$

crystal. Each measured ratio was greater than the calculated value with the ± (555) intensity ratio in closest agreement. Any difference in perfection would have a smaller effect on higher-order reflections because the dynamical and kinematic theories predict the same integrated intensities in the limit of weak reflections. However, because the (222) and $(\bar{2}\bar{2}\bar{2})$ profiles were indistinguishable, these differences in perfection had a negligible effect in the fluorescence profiles. Therefore the differences in the (111) and $(\bar{1}\bar{1}\bar{1})$ profiles must have resulted from the difference in the internal wave field motion relative to the atomic planes.

The calculated profiles were obtained neglecting the imaginary terms in the atomic scattering factors. If the imaginary terms had been included, the magnitudes of F_{111} and $F_{\bar{1}\bar{1}\bar{1}}$ for Cu $K\alpha$ radiation would differ by less than 0.5%. More importantly, the phases of the structure factors would be changed. For the (111) reflection, the angle $\arctan(f_P/f_{Ga})$ in Eqs. (7)–(9) would become $\arctan[(f_P+\Delta f''_{Ga})/(f_{Ga}-\Delta f''_P)]$. These angles differ by less than 2°, justifying the approximations for the cases treated here.

SUMMARY AND CONCLUSIONS

The dynamical theory of diffraction has been applied to a noncentrosymmetric crystal and the details of the internal wave field were calculated for the symmetric Bragg case. The maximal and minimal surfaces of the internal field intensity were shown to move normal to the surface and into the crystal as the region of total reflection is scanned from a low to a high angle of incidence. Using fluorescence from the phosphorus atoms in GaP, the position of the internal wave field as a function of incident angle was monitored. The experimental fluorescence profiles were obtained during symmetric Bragg reflections from the (111), $(\bar{1}\bar{1}\bar{1})$, (222), and $(\bar{2}\bar{2}\bar{2})$ reflections from GaP. The qualitative features of the experimental profiles agree with calculated profiles and can be used to determine the polarity of the crystal. This new technique for determining polarity is significant in that it does not depend upon anomalous scattering contributions, as have all previous determinations.[15,16,18]

A polarity determination for the same GaP crystal using the conventional anomalous dispersion technique yielded results consistent with the fluorescence technique. This experimental check of the x-ray anomalous dispersion technique refutes claims that have been made that x-ray absolute configurations determined by anomalous scattering are wrong.[7] The application of the anomalous scattering to neutron diffraction was recently checked[8] and the results reported here may be viewed as a confirmation of the anomalous dispersion technique for x-ray diffraction.

The movement of the maximal surfaces of the internal wave field generated during a Bragg reflection has been monitored on a finer atomic scale than has been done previously. The application of this technique, although restricted to crystals of high perfection, allows the determination of the arrangement of atoms in crystals in a new and direct way.

ACKNOWLEDGMENTS

The author wishes to thank Dr. W. Wagner for providing the prepared GaP samples, and Professor B. W. Batterman for helpful discussions. Batterman's suggestion that long-wavelength fluorescence be monitored proved invaluable to the success of the experiment.

This work was supported in part by a Cottrell Research Grant from the Research Corporation, and by the NSF, University Science Development Grant No. DID68-00431-A03.

[1] W. H. Zachariasen, *Theory of x-ray Diffraction in Crystals* (Wiley, New York, 1945).
[2] R. W. James, *The Optical Principles of the Diffraction of x rays* (Bell, London, 1950).
[3] B. W. Batterman and H. Cole, Rev. Mod. Phys. 36, 681 (1964).
[4] B. W. Batterman, Phys. Rev. 133, A759 (1964).
[5] B. W. Batterman, Phys. Rev. Lett. 22, 703 (1969).
[6] J. A. Golovchenko, B. W. Batterman, and W. L. Brown, Phys. Rev. B 10, 4239 (1974).
[7] J. Tanaka, F. Ozeki-Minakato, and M. Nagakawa, Spectrochim. Acta A 29, 897 (1972).
[8] G. P. Felcher and S. W. Peterson, Acta Crystallogr. A 31, 76 (1975).
[9] M. Kohler, Ann. Phys. (Leipz.) 18, 265 (1933).
[10] Nodal surfaces exist only for the σ polarization state, when $P=1$ and $|E_H/E_0|=1$ in the region of total reflection. For the π polarization state and outside the region of total reflection, minimal surfaces still exist.
[11] *International Tables for x-ray Crystallography* (Kynoch Press, Birmingham, 1962), Vol. III.
[12] E. D. Pierron, D. L. Parker, and J. B. McNeely, J. Appl. Phys. 38, 4669 (1967).
[13] D. T. Cromer and J. T. Waber, Acta Crystallogr. 18, 104 (1965).
[14] D. T. Cromer and D. Liberman, J. Chem. Phys. 53, 1891 (1970).
[15] D. Coster, K. S. Knol, and J. A. Prinz, Z. Phys. 63, 345 (1930).
[16] H. Cole and N. R. Stemple, J. Appl. Phys. 33, 2227 (1962).
[17] J. R. Patel, R. S. Wagner, and S. Moss, Acta Metall. 10, 759 (1962).
[18] S. Hosoya and T. Fukamachi, J. Appl. Crystallogr. 6, 396 (1973). [An important erratum to this paper is to be published; page 396, column two, line 1: $(\frac{3}{3}, \frac{3}{4}, \frac{3}{3})$ should read $(\frac{1}{4}, \frac{1}{4}, \frac{1}{4})$].